Mechanisms of Electrochemical N_2 Splitting by a Molybdenum Pincer Complex

Quinton J. Bruch,[†] Santanu Malakar,[‡] Alan S. Goldman,[‡] Alexander J. M. Miller[†*]

[†] *Department of Chemistry, University of North Carolina at Chapel Hill, Chapel Hill, North Carolina 27599–3290, United States*

[‡] *Department of Chemistry and Chemical Biology, Rutgers, The State University of New Jersey, New Jersey, 08903, United States*

ABSTRACT: Molybdenum complexes supported by tridentate pincer ligands are exceptional catalysts for dinitrogen fixation using chemical reductants, but little is known about their prospects for electrochemical reduction of dinitrogen. The viability of electrochemical N_2 binding and splitting by a molybdenum(III) pincer complex, (^{py}PNP)MoBr$_3$ (^{py}PNP = 2,6-bis(^{t}Bu$_2$PCH$_2$)-C$_5$H$_3$N)), is established in this work, providing a foundation for a detailed mechanistic study of electrode-driven formation of the nitride complex (^{py}PNP)Mo(N)Br. Electrochemical kinetic analysis, optical and vibrational spectroelectrochemical monitoring, and computational studies point to two concurrent reaction pathways: in the reaction–diffusion layer near the electrode surface, the molybdenum(III) precursor is reduced by 2e^- and generates a bimetallic molybdenum(I) Mo$_2$(μ-N$_2$) species capable of N–N bond scission; in the bulk solution away from the electrode surface, over-reduced molybdenum(0) species undergo chemical redox reactions via comproportionation to generate the same bimetallic molybdenum(I) species capable of N_2 cleavage. The comproportionation reactions reveal the surprising intermediacy of dimolybdenum(0) complex *trans,trans*-[(^{py}PNP)Mo(N$_2$)$_2$](μ-N$_2$) in N_2 splitting pathways. The same "over-reduced" molybdenum(0) species was also found to cleave N_2 upon addition of lutidinium, an acid frequently used in catalytic reduction of dinitrogen.

1. INTRODUCTION

The fixation of dinitrogen as ammonia via the Haber-Bosch process (HB) is a critical industrial transformation that underpins the production of synthetic fertilizers. The cost of a process that supports roughly 50% of the global food supply[1,2] is an enormous energy requirement: ca. 2% of annual energy expenditures worldwide. Furthermore, HB relies on H_2 sourced from fossil fuels resulting in ca. 2% of annual CO_2 emissions.[3] This combination of an over-reliance on fossil fuels and massive energy input requirements contextualized against the backdrop of ongoing climate crises has made the pursuit of sustainable industrial NH_3 production a major scientific challenge.

One HB alternative is a fully electrochemical approach that combines N_2 and H^+ and e^- equivalents derived from water oxidation (**Scheme 1**, top). This approach not only removes the reliance on fossil fuels, but could decentralize NH_3 production and thus avoid requisite CO_2 emissions associated with ammonia distribution.[4,5]

Scheme 1. Comparison of electrochemical and chemical approaches to dinitrogen fixation ("Red" is a chemical reductant).

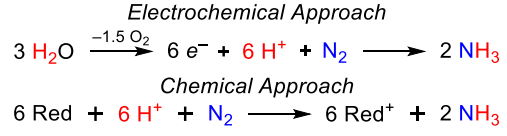

To date, however, the prevailing approach has focused on molecular N_2 fixation catalysts driven by an excess of chemical reductants (**Scheme 1**, bottom). Molybdenum catalysts have played a particularly prominent role, starting with Schrock's seminal work with trisamido-amine systems[6] and ongoing breakthroughs by Nishibayashi, and others.[7–10] One unifying theme in these molecular catalyst studies is that they all utilize excess chemical reductants under the auspices of later transitioning to electrode-mediated reductions. However, there are very few examples of electrochemical N_2 reduction.[11–17]

The prototypical (^{py}PNP)Mo catalysts (^{py}PNP = 2,6-bis(^{t}Bu$_2$PCH$_2$)-C$_5$H$_3$N)) would be an ideal starting point for electrochemical exploration due to their high catalytic activity. The first reported (^{py}PNP)Mo catalyst, the dimolybdenum(0) [(^{py}PNP)Mo(N$_2$)$_4$]$_2$(μ-N$_2$) (**1**, **Scheme 2A**),[18] has been proposed to undergo distal protonation at one of the terminal N_2 ligands to initiate catalysis via a classical "Chatt cycle" mechanism.[19–22] Catalysts developed later, such as the monometallic molybdenum(III) complex (^{py}PNP)MoBr$_3$ (**2**, **Scheme 2A**) exhibit higher activity under the same conditions (**Scheme 2B**) and have been proposed to proceed via the N_2 cleavage mechanism in which a bimetallic molybdenum(I) Mo$_2$(μ-N$_2$) intermediate precedes formation of a Mo(N) and subsequent N–H bond formation. [23,24]

The high yields and catalytic activity observed under the N_2 cleavage pathway indicate that **2** would be a prime candidate for investigation of electrochemical reactivity. However, while redox potentials of several (^{py}PNP)Mo species have been reported to date,[22,23] the electrochemical behavior of **2** remains unexplored. It is also unclear whether the chemical reactivity of **2** will readily translate to an electrochemical approach, or if there are unique features of

electrochemically driven N_2 activation and splitting for these molybdenum catalysts.

Scheme 2. (A) Examples of active N_2 fixation catalysts supported by the (^{py}PNP) ligand. (B) Comparison of catalyst activity in N_2 fixation under identical conditions. Equivalents of reagents are per Mo center.[23]

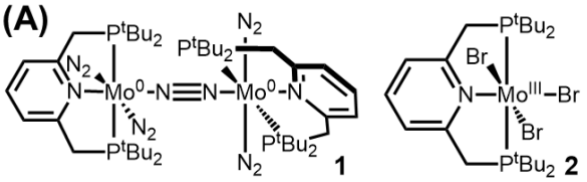

Catalyst	TON	TOF (h^{-1})
1	13	12
2	31	29

In this study, we demonstrate the viability of electroreductive N_2 splitting by (^{py}PNP)$MoBr_3$ (**2**) and use electroanalytical methods and a suite of spectroelectrochemistry experiments to establish key features of the electrochemical mechanism of N_2 activation and splitting into nitride complexes. Herein we identify two concurrent pathways which rely on *monometallic-bimetallic equilibria* to gate reactivity at the electrode surface and minimize the necessary applied potentials. We also establish the essential role of *chemical redox reactions* far from the electrode surface, which activate the *electrochemically produced* "over-reduced" Mo^0 complex **1** towards N_2 splitting. Given that complex **1** was previously thought to follow an independent path of N_2 reduction that does not rely on N_2 cleavage, its observation during electrochemical N_2 splitting helps identify a potentially broader role of Mo^0 complexes as electron reservoirs in both chemical and electrochemical N_2 reduction to NH_3.

2. RESULTS AND DISCUSSION

2.1 Electrochemical reactivity of (^{py}PNP)$MoBr_3$ under Ar and N_2. Initial cyclic voltammograms (CVs) of (^{py}PNP)$MoBr_3$ (**2**) were recorded under Ar and N_2, revealing a clear impact of the atmosphere on the electrochemical behavior (**Figure 1A-1B**). Therefore, the behavior of **2** was studied in more detail under both Ar and N_2 to elucidate when and how chemical reactions with N_2 occur upon reduction. In this section we discuss the behavior of the first reduction feature, see SI Section VIII for investigation of additional reduction events.

CVs of **2** under Ar at scan rates (ν) below 10 V/s present a completely irreversible reduction around –1.81 V (all potentials are reported versus $Fc^{+/0}$ unless otherwise stated) that shifts anodically at slower scan rates (**Figure 1A**). The CVs also contain an irreversible oxidation (ca. –1.27 V) that is only present in the return sweep and shifts cathodically at slower scan rates. At ν ≥ 20 V/s, the reduction feature becomes partially reversible ($E_{1/2}$ ≈ –1.85 V, **Figure S38**), with peak-to-peak separations consistent with a $1e^-$ process (ΔE_p(Mo) = 299 mV, ΔE_p($FeCp^*_2$) = 261 mV).

The observed electrochemical behavior is indicative of an EC process (electrochemical step followed by chemical step) involving $1e^-$ reduction of **2** to form [(^{py}PNP)$MoBr_3$]$^-$ (**2**$^-$, **Figure 1D**), which would dissociate Br^- to yield (^{py}PNP)$MoBr_2$ (**3**, **Figure 1D**) in a chemical step (C_{Br}). The rate constant for this process was estimated using the $E_{1/2}$ and the scan rate-dependent shift in E_{pc} revealing a forward estimated rate (k_f) of C_{Br} to be 400 s^{-1} ± 100 s^{-1} (**Figure S39**).[25,26] This rate constant is comparable to chloride dissociation from reduced [(L)$ReCl_2$]$^-$ species (L = amido(diphosphine)) prior to N_2 splitting (100 < k_f < 1000 s^{-1}).[13,16]

The assigned C_{Br} step could be further confirmed by recording CVs of **2** under Ar in the presence of increasing concentrations of Br^-. While the reduction did not change significantly at slow scan rates as a function of bromide concentration (**Figure 1C**), the return oxidation feature became more reversible. Surprisingly, however, the return oxidation is still irreversible at faster scan rates (1 V/s, **Figure S42**) even in the presence of 100 equivalents of Br^-. This suggests the electrochemical oxidation of **3** proceeds by a CE mechanism wherein Br^- coordination forms a small equilibrium amount of **2**$^-$ that is then oxidized back to **2** (see SI Section VIII for more details).

Digital simulations also support an EC-CE mechanism. Suitable agreement required a model in which reduction of **2** to **3** is followed by THF binding to generate (^{py}PNP)$MoBr_2$(THF) (**3-THF**). The reversible ligand substitution of Br^- for THF (**Figure 1D**, C_{THF}) is experimentally estimated to thermodynamically favor **3-THF** by –2 kcal/mol (see SI Section VIII for more details). Computations further support the C_{Br} step, as DFT predicts Br^- loss to be exergonic (computed ΔG°_{CBr} = –2 kcal/mol, THF binding in C_{THF} was computed to be uphill, ΔG°_{CTHF} = 15 kcal/mol, see SI Section XII). The iodide analogue of **3**, (^{py}PNP)MoI_2, was also recently synthesized by reducing (^{py}PNP)MoI_3 with $CoCp^*_2$ (Cp* = pentamethylcyclopentadienyl) under Ar.[27] Identification of the loss of bromide upon reduction is important, as it provides a vacant coordination site for N_2 binding.

Moving to an N_2 atmosphere has a marked impact on the electrochemical response. Under N_2, the first reduction feature of **2** was found to be partially reversible at fast scan rates ($E_{1/2}$ ≈ –1.86 V at 30 V/s, **Figure S32**). At moderate scan rates (5 ≤ ν ≤ 10 V/s), fully irreversible EC behavior was observed with an experimentally determined k_f of 370 s^{-1} ± 100 s^{-1} (see SI Section VIII). The estimated $E_{1/2}$ at fast scan rates and the rate constant are within error of the values determined under Ar ($E_{1/2}$ ≈ –1.85 V, k_f = 400 s^{-1} ± 100 s^{-1}), suggesting that C_{Br} is the first chemical step under

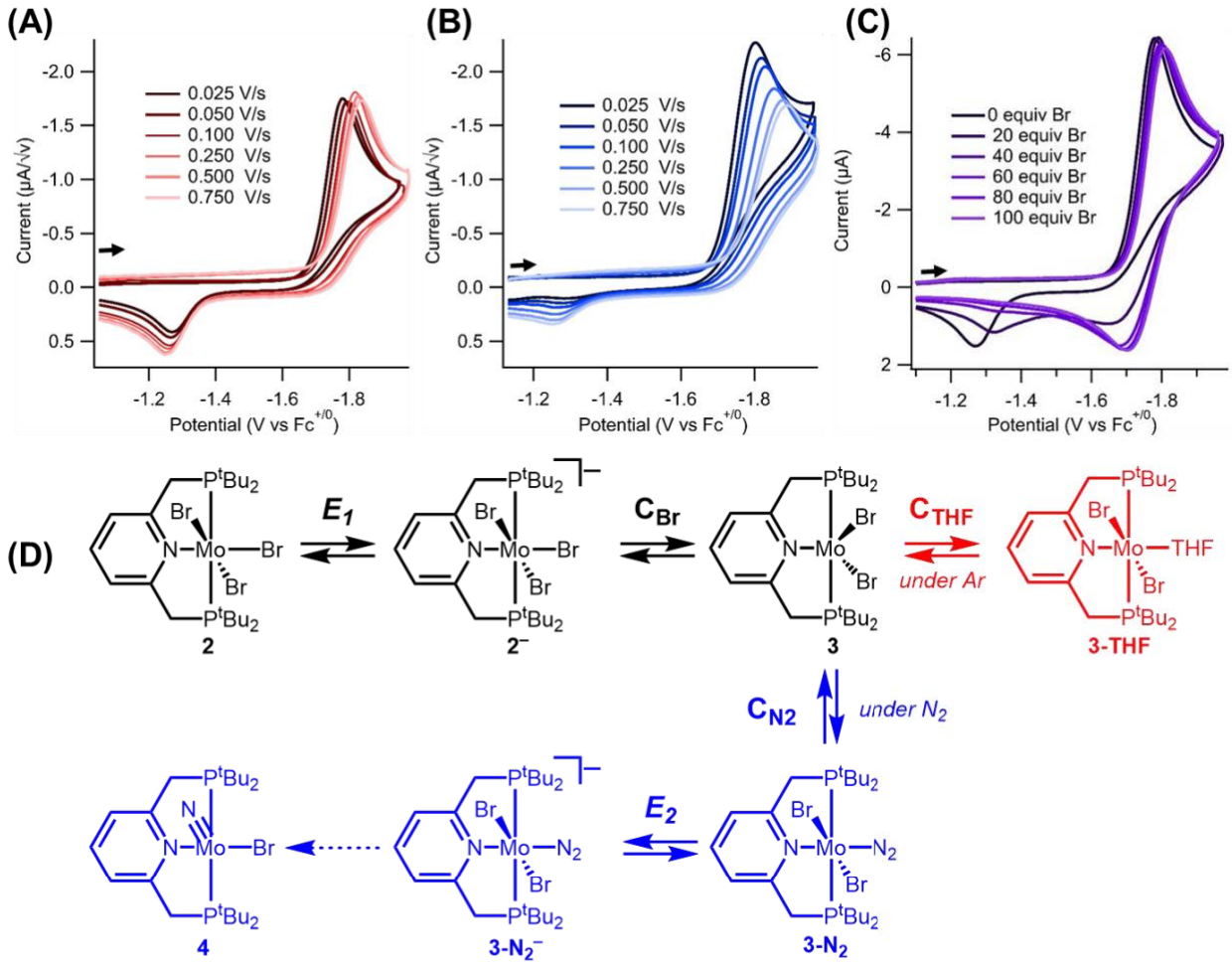

Figure 1. CVs of 1 mM (^{py}PNP)MoBr$_3$ (**2**) in 0.2 M [^{n}Bu$_4$N][PF$_6$] in THF (A) under Ar sweeping cathodically at varying scan rates, (B) under N_2 sweeping cathodically at varying scan rates, and (C) under Ar sweeping cathodically at 0.025 V/s with varying [Br$^-$]. (D) Proposed mechanisms upon reduction of **2** under Ar (top, red) and under N_2 (bottom, blue). $E_2 > E_1$.

N_2. At scan rates ≤ 1V/s, E_{pc} shifted anodically and the scan-rate-normalized cathodic peak current ($i_{pc}/\sqrt{v}$) increased (**Figure 1B**) suggesting additional reactivity with N_2. Based on the proposed structure of **3**, initial N_2 binding to yield (^{py}PNP)MoBr$_2$(N_2) (**3-N$_2$**, **Figure 1D**) is reasonable, with N_2 binding computed to be slightly endergonic (6 or 7 kcal/mol to form the *cis* or *trans* isomer, respectively). The observed increase in $i_{pc}/\sqrt{v}$ indicates that more than 1e^- during the first reduction feature under N_2, likely due to additional reductions of **3-N$_2$** once it forms at the electrode surface via "potential inversion" (E_2>E_1). This behavior can be attributed to the π-acidic nature of the N_2 ligand causing dramatic anodic shifts in reduction potentials of M(N_2) species relative to M.[13,16,28-34]

The voltammetric studies together provide clear evidence for the initial sequence shown in **Figure 1D**, with electroreduction-induced bromide dissociation followed by N_2 association to form a dinitrogen complex that undergoes additional reduction(s).

2.2 Electrochemical N_2 Splitting. To establish the products of the electroreduction under N_2, controlled potential electrolysis (CPE) was carried out on a 4 mM solution of **2** in THF under N_2 near the first reduction peak potential (E_{appl} = –1.89 V vs Fc$^{+/0}$). Over the course of the electrolysis, two 'zones' of current response were observed and corresponded to color changes from orange to blue to green as the charge equivalent of 2e^- per Mo center was passed (**Figure 2B**). Analysis of the resulting catholyte revealed the desired molybdenum nitride product (^{py}PNP)Mo(N)Br (**4, Figure 2A**) was formed in 41% ± 1% yield according to ^{1}H NMR spectroscopy (Figures S22-S23). In addition to **4**, the over-reduced Mo^0 species [(^{py}PNP)Mo(N_2)$_4$]$_2$(μ-N_2) (**1**) could also be detected in trace quantities (< 2%), but no other products could be identified. The 41% yield of nitride is similar to other reports of electrochemical N_2 splitting.[13,16]

Having demonstrated that electrochemical N_2 splitting was feasible, N_2 splitting with chemical reductants was targeted next. CoCp*$_2$ was selected due to the similarity between its reduction potential ($E_{1/2}$ = –1.85 V in THF, **Table S1**) and E_{appl}. Addition of 3.3 equiv of reductant to **2** in THF-d_8 results in the formation of an intensely blue solution and yellow-brown insoluble [CoCp*$_2$][Br]. After 16 h, the solution remained an intensely blue color and the molybdenum nitride species **4** was detected in 20% yield by

^{1}H NMR spectroscopy. The bimetallic Mo^0 **1** was not detected, but free ^{py}PNP ligand was found (6% yield) as well as trace unidentified diamagnetic species (14%). Excitingly, the yield of the desired Mo(N) was higher during electrochemical reductions.

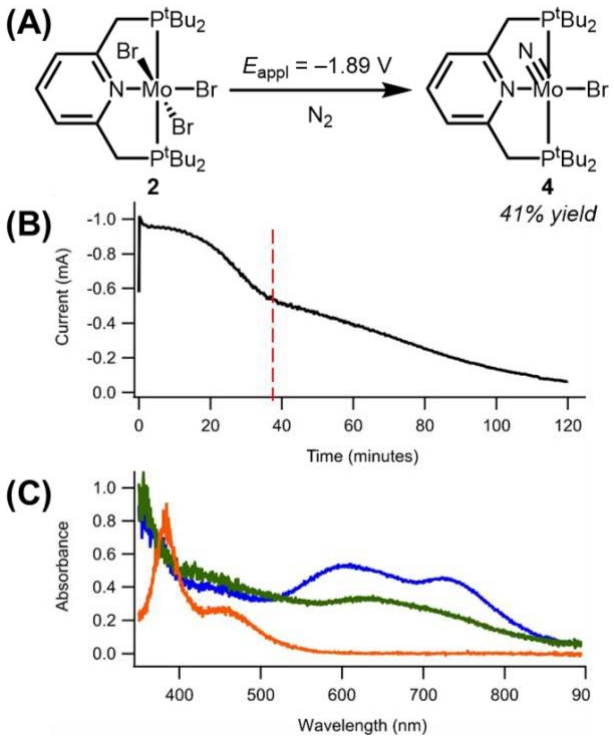

Figure 2. (A) Electrochemical N_2 splitting upon reduction of (^{py}PNP)$MoBr_3$ (**2**) to yield (^{py}PNP)Mo(N)Br (**4**). (B) CPE trace during the reduction of **2** (4 mM) in THF (0.2 M [^{n}Bu$_4$][PF_6]) under an N_2 atmosphere. Red dashed line marks the start of the color change from blue to green. (C) UV-Vis spectra of the bulk solution during the CPE reduction of **2** at 0 min (orange), 45 min (blue), and 120 min (green).

The appearance of two "zones" during the CPE and two distinct color changes hints at the formation of detectable intermediates. To search for and characterize these intermediates, CPE of **2** was carried out under the same conditions used above but with aliquots taken from the bulk solution for IR and UV-Vis spectroscopic measurements every 5-10 minutes.

During the first "zone", the solution turns from orange to blue and UV-Vis analysis revealed the formation of new absorbances (λ_{max} = 600 and 729 nm) over the first 45 min of electrolysis (**Figure 2C**, blue). During this time, charge correlating to 1.3 e^- per Mo was passed, suggesting the blue-colored intermediate is a one-electron reduction product. Continued monitoring (45 to 120 minutes) revealed the intermediate to be transient, as yet another species with a broad shoulder centered at 633 nm was detected as the solution turned from dark blue to dark green as an additional ca. 0.7 e^- (2.0 e^- equiv total) were passed (**Figure 2C**, green). Throughout the course of the experiment, no terminal N_2 stretches were detected by IR spectroscopy.

2.3 Synthesis and Electrochemical Reactivity of an Isolable Mo^{II} Intermediate. To further investigate the initial intermediate formed, one-electron reduction of **2** was explored using chemical reductants. Addition of 1 equiv of $CoCp^*_2$ to **2** at –30 ˚C in THF resulted in rapid formation of a dark red solution that slowly turned dark blue over the course of 30 min at –30 ˚C (**Scheme 3**). Analysis of the isolated solid via UV-Vis revealed nearly identical absorbance features (λ_{max} = 606 and 730 nm) to those detected during electrochemical reduction (**Figure 2C, blue**).

Scheme 3. Synthesis of *trans,trans*-[(^{py}PNP)$MoBr_2$]$_2$(μ-N_2) (**5^{t,t}**).

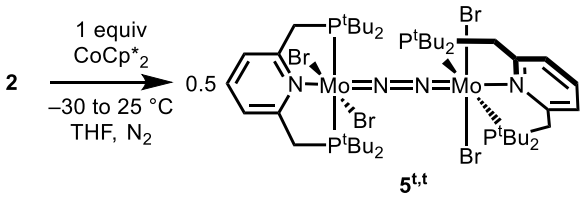

NMR spectroscopy in THF-d_8 revealed the species to be paramagnetic and no (^{py}PNP)Mo(N)Br was detected. Evans Method measurements yielded a solution magnetic moment, μ_{eff}, of 5.4, which is similar to the expected spin only value of a quintet state ($\mu_{s.o.}$ = 4.9). Saturated THF solutions of the blue solid revealed no terminal ν_{NN} stretches by IR spectroscopy while resonance Raman (rR) spectra contained features at 1595 and 1751 cm^{-1}. The feature at 1751 cm^{-1} was assigned to a bridging N_2 ligand while the stretch at 1595 cm^{-1} was assigned to the (^{py}PNP) ligand (*vide infra*).[35,36] Single crystals grown via vapor diffusion of pentane into a saturated toluene solution at 25 ˚C allowed for unambiguous assignment as the N_2-bridged bimetallic Mo^{II} species, *trans,trans*-[(^{py}PNP)$Mo(Br)_2$]$_2$(μ-N_2) (**5^{t,t}**, **Figure 3**). The solid state structure of **5^{t,t}** is similar to the tetrachloride analogue,[37] and contains a modestly activated N_2 ligand (N–N bond distance of 1.160(3) Å versus 1.110 Å in free N_2[38]) which aligns with the measured ν_{NN} stretching frequency.[38]

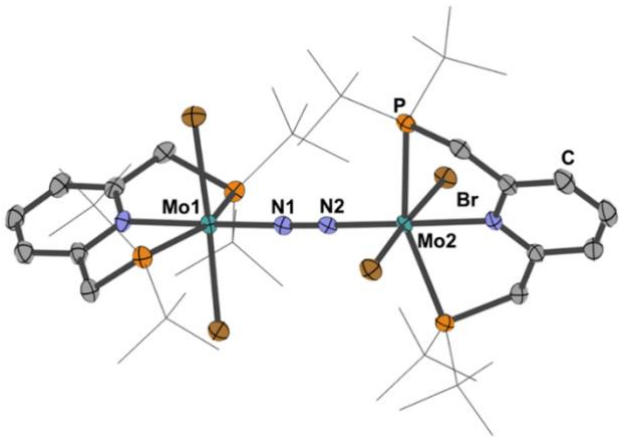

Figure 3. Structural representation of *trans,trans*-[(^{py}PNP)MoBr$_2$]$_2$(μ-N$_2$) (**5^{t,t}**) from singe crystal X-ray diffraction with ellipsoids set at 50% occupancy. For clarity, hydrogen atoms were omitted and ^{t}Bu substituents are wire-framed for improved visibility. Select bond distances (Å): Mo1–N1: 1.926(2); N1–N2: 1.160(3); Mo2–N2: 1.926(3). Select angle (°): Mo1-N1-N2: 178.7(2), Mo2-N2-N1: (175.9(2). See SI Section XIII for more details.

Although dimolybdenum(II) complex **5^{t,t}** contains the desired end-on bridging N$_2$ binding mode needed for N$_2$ splitting, **5^{t,t}** is stable both in the solid and solution state for weeks at a time. The N$_2$-bridged complex **5^{t,t}** is therefore not kinetically competent for N$_2$ splitting on the ca. 2 h timescale of the CPE experiments. The observed lack of reactivity is unsurprising, as the strict electronic structure requirements of N$_2$ splitting should only be satisfied by a dimolybdenum(I) complex.[39-42]

Having ruled out direct N$_2$ splitting from **5^{t,t}** itself, we hypothesized that further reduction would be needed to furnish the nitride product. The electrochemical behavior of the proposed intermediate was therefore explored next. Starting with CVs of **5^{t,t}** under an N$_2$ atmosphere, sweeping reductively revealed a minor feature at ca. –1.84 V that passed significantly less current than the major reduction feature around –2.16 V (**Figure 4A**). The minor feature at –1.84 V is similar to where the reduction of **2** occurs; however, trace **2** could be ruled out as an impurity based on comparisons of CVs of **2** and **5^{t,t}** under Ar where it is clear that the return oxidation feature at ca. –1.27 V is absent (**Figure S54**). Scan rate dependency studies of **5^{t,t}** under N$_2$ and Ar revealed the major reduction feature at ca. –2.16 V to be an EC process under Ar and an EC$_{N2}$E process under N$_2$ (**Figure 4A**, see SI section IX for more details). These studies also revealed that the prewave feature at ca. –1.84 V shifted anodically while $i_{pc}/\sqrt{\nu}$ increased at slower scan rates, which along with relatively small amount of charge passed are hallmark signs of a CE process. Based on the structure of **5^{t,t}**, we attribute the chemical step to a dissociation of the bimetallic **5^{t,t}** coupled with binding of N$_2$ to yield the monometallic species **3-N$_2$**. This monometallic-bimetallic equilibrium shown in **Figure 4B** was computationally explored, and found to be only modestly endergonic at room temperature ($\Delta G^\circ_{\mathbf{5t,t},diss}$ = 5 kcal/mol, see SI Section XII).

Considering the CVs in **Figure 4** within the context of CPE-driven N$_2$ splitting, we found that the potential applied during CPE (–1.89 V) aligns with the *prewave* CE feature of **5^{t,t}** (–1.84 V), rather than the main reduction of **5^{t,t}** (–2.16 V). Therefore, CPE of **2** was carried out at an applied potential of –2.11 V under N$_2$, a potential where intermediate **5^{t,t}** would be reduced rapidly (**Table 1**). Surprisingly, the yield of the Mo(N) product **4** *decreased* from 41% to 17% and several unidentified diamagnetic Mo products were observed (**Figure S26**).

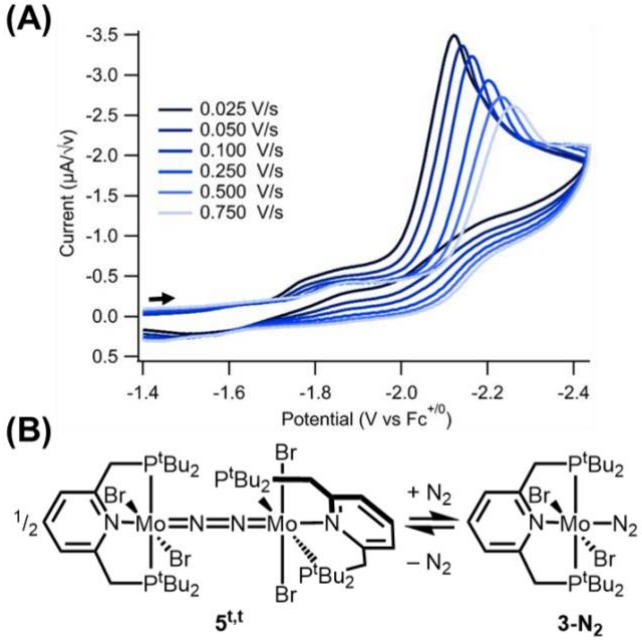

Figure 4. (A) CVs of of 1 mM *trans,trans*-[(^{py}PNP)MoBr$_2$]$_2$(μ-N$_2$) (**5^{t,t}**) under N$_2$ sweeping cathodically at varying scan rates. (B) Proposed monometallic-bimetallic equilibrium as the chemical step in the CE prewave process.

To further probe the potential dependence of N$_2$ splitting, CPE of 2 mM solutions of **5^{t,t}** ([Mo]$_{total}$ = 4 mM) to generate **4** was carried out under N$_2$ at the E_{pc} of both the prewave CE feature and the main reduction feature (**Table 1**). Notably, yields of **4** were lower from the reduction of the apparent intermediate **5^{t,t}** than from the direct reduction of **2** and, once again, at milder potentials, the yield of **4** was substantially higher (22% versus 3%, at -1.89 V and -2.11 V respectively, **Table 1**). Finally, because **5^{t,t}** contains a pre-coordinated N$_2$ ligand, CPE under Ar could also yield the Mo(N) product. Remarkably, the electrochemical yields of **4** upon electrolysis of **5^{t,t}** under Ar were markedly higher than under N$_2$ (41% vs. 22% at –1.89 V, 43% v 3% at –2.11 V).

Table 1. Electrochemical reduction of (^{py}PNP)Mo(N)Br (**4**) under varying conditions.

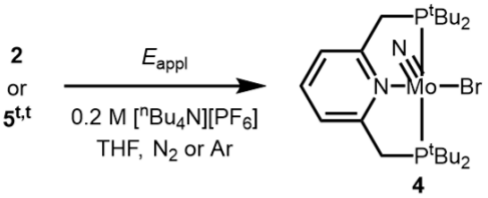

(^{py}PNP)Mo precursor	Atm	E_{appl}	% Yield of (^{py}PNP)Mo(N)Br[a]
2	N$_2$	–1.89 V	41% ± 1%
2	N$_2$	–2.11 V	17%
2	Ar	–1.89 V	0%
5^{t,t}	N$_2$	–1.89 V	22%
5^{t,t}	N$_2$	–2.11 V	3%
5^{t,t}	Ar	–1.89 V	42%
5^{t,t}	Ar	–2.11 V	43%

[a]Yields of **4** were calculated using the concentration of **4** determined by ^{1}H NMR spectroscopy and the total concentration of Mo starting material used (see SI Section VI for an example calculation).

The yields of **4** reported in **Table 1** clearly demonstrate a strong dependence on all three parameters: (^{py}PNP)Mo precursor, atmosphere, and applied potential. Under Ar, N_2 cleavage is only observed when it is pre-incorporated in **5^{t,t}**. Intriguingly, the yields of **4** from **5^{t,t}** under Ar are not impacted by applied potential *and* they are substantially higher than under N_2. This is consistent with electrochemical reduction of **5^{t,t}** (or the monometallic analogue **3-N$_2$**) to form nitride **4** at the electrode surface. The detrimental impact of N_2 when starting from **5^{t,t}** suggests that the ability for reduced Mo species to interact with additional N_2 molecules may lead to deleterious side reactions.

2.4 Spectroelectrochemical Identification of Low Valent Mo^0 Intermediates. To directly probe the Mo species formed at the surface of the electrode,

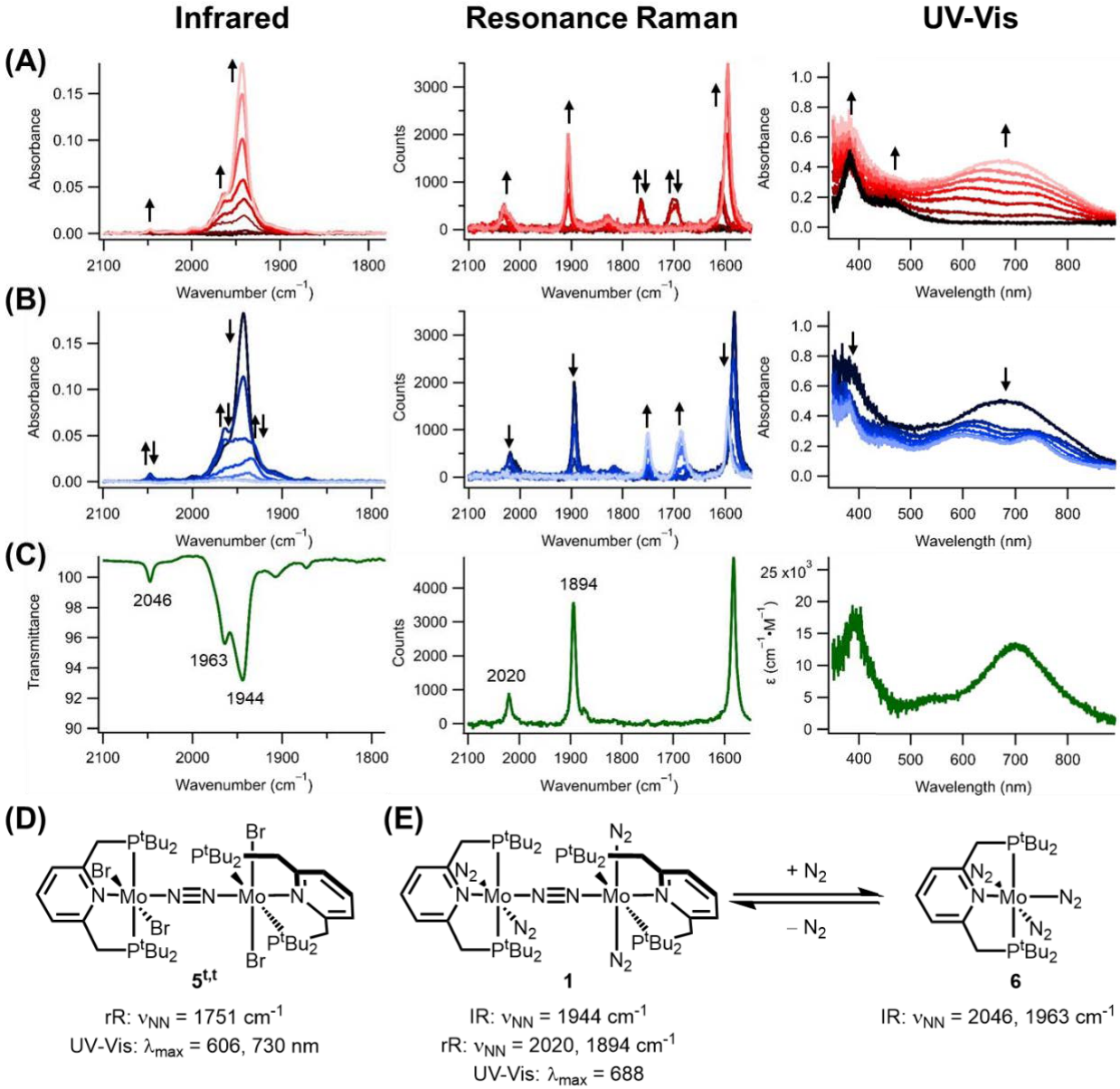

Figure 5. (A) Stepped potential spectroelectrochemical experiments from –0.5 to –1.5 V (vs $Ag^{+/0}$) of 4 mM (^{py}PNP)$MoBr_3$ (**2**) in 0.2 M [^{n}Bu$_4$][PF_6] in THF under N_2 monitoring by IR (left) rR (middle) and UV-Vis (right). (B) Monitoring the consumption of electrode-generated [(^{py}PNP)Mo(N_2)$_2$]$_2$(μ-N_2) (**1**) over time, recording spectra every 5 minutes by IR (left, 30 min), rR (middle, 40 min), and UV-Vis (right, 30 min). (C) Authentic IR, rR, and UV-Vis of freshly prepared *trans,trans*-[(^{py}PNP)Mo(N_2)$_2$]$_2$(μ-N_2) (**1**). Peaks marked with arrows pointing in both directions are transient. (D) Spectroscopic data attributed to *trans,trans*-[(^{py}PNP)$MoBr_2$]$_2$(μ-N_2) (**5^{t,t}**). (E) Equilibrium between [(^{py}PNP)Mo(N_2)$_4$]$_2$(μ-N_2) (**1**) and (^{py}PNP)Mo(N_2)$_3$ **6** and spectroscopic data assigned to each species. All potential steps are in –0.1 V increments and potentials were held for 120 seconds. Peaks marked with arrows pointing in both directions are transient.

spectroelectrochemistry (SEC) studies were carried out on 4 mM solutions of **2** in 0.2 M [^{n}Bu$_4$][PF$_6$] solutions in THF under an N_2 atmosphere. A thin-layer transmission cell with a Au mini-grid working electrode was used for both IR and rR spectroeletrochemistry,[43] and a short pathlength cuvette fitted with a honeycomb Au working electrode was used for UV-Vis spectroelectrochemistry. In all cases (IR, rR, UV-Vis) a progressively more negative potential was applied, stepping –0.1 V every 120 seconds.

Monitoring the products formed at the surface of the electrode by IR spectroscopy revealed the formation of a dominant feature at 1944 cm^{-1} as well as a shoulder at 1963 cm^{-1} and a minor stretch at 2043 cm^{-1} (**Figure 5A**). While this clearly indicates the formation of terminal Mo(N_2) species, the generation of known intermediates such as **5^{t,t}** featuring symmetric bridging N_2 ligands would not be detected, as they are IR silent. Therefore, the rR spectrum was also monitored over the same potential range. Using a Raman microscope equipped with a 633 nm laser, electrolysis of **2** resulted in the initial formation of stretches at 1595, 1684, and 1751 cm^{-1} (**Figure 5A**). The features at 1595 and 1751 cm^{-1} clearly align with the Mo^{II} species **5^{t,t}** (**Figure 5D**), while the feature at 1680 cm^{-1} is likely an isomer of **5^{t,t}**, as the shift to more activated N_2 stretches has been previously observed in Re$_2$(μ-N_2) complexes and is computational predicted upon isomerization of *trans,trans* M$_2$(μ-N_2) species.[42,44] Additionally, monitoring the chemical reduction of **2** with 1 equiv of CoCp*$_2$ via rR revealed a minor feature at ca. 1680 cm^{-1} that decayed alongside concomitant growth of the feature at 1751 cm^{-1} that corresponds to **5^{t,t}** (**Figure S9**). Ultimately, these bimetallic Mo^{II} species proved to be transient, as at more negative potentials features at 1583, 1894, and 2020 cm^{-1} dominated the rR spectrum (**Figure 5A**). Repeating these experiments under an Ar atmosphere led to no IR features from 2200 to 1800 cm^{-1} and only a rR stretch at 1574 cm^{-1} which was attributed to the ^{py}PNP ligand (**Figure S72**).[35,36] While starting solutions of **2** do not show rR stretches in this region, we attribute this to the inability of **2** to efficiently absorb 633 nm light (vide infra).

UV-Vis SEC carried out under identical conditions resulted in increased absorbance between 400 and 900 nm that coalesced into a single broad feature at 684 nm (**Figure 5A**). It is important to note that the UV-vis spectra acquired using the honeycomb electrode, which provides insight into the species in the vicinity of the surface of the electrode, are distinct from the spectra of aliquots taken during a standard bulk electrolysis experiment (see above). The major species with λ_{max} = 684 nm was confirmed to be a Mo(N_2) complex, as UV-Vis SEC under Ar revealed new λ_{max} features at 354 nm and a broad shoulder centered at 500 nm that slowly decays into the red (**Figure S64**). Approximately 85% of the Mo-containing species can be accounted for at any given time in the UV-vis SEC experiments, which provides good evidence that the early stages of the reaction proceed cleanly enough to carry out a meaningful mechanistic study despite the 41% yield of nitride in exhaustive preparative electrolyses.

Over the course of the spectroelectrochemical measurements, all three spectroscopic probes are consistent with formation of the dimolybdenum(0) complex **1** as the dominant species at the electrode surface: [(^{py}PNP)Mo(N_2)$_2$]$_2$(μ-N_2) has a reported IR stretch at 1944 cm^{-1} (dominant IR SEC feature) and a rR stretch at 1894 cm^{-1} (dominant rR SEC feature).[18] Furthermore, **1** was prepared by reducing **2** with 3 equiv of KC_8 and authentic spectra closely matched all SEC data (**Figure 5C**). Unexpectedly, the authentic spectra of **1** also contained features at 1963 and 2046 cm^{-1}, aligning with minor features observed during IR SEC experiments. We assign these features to a monometallic species, (^{py}PNP)Mo(N_2)$_3$ (**6**, **Figure 5E**) because IR spectra of recrystallized **1** under N_2 showed equilibration between features at 2047, 1963, and 1942 cm^{-1} while under Ar no change was observed (**Figure S8**). Similar monometallic-bimetallic equilibria have been previously reported in a number of d^6 (pincer)Mo(N_2) systems,[22,45,46] and the **1**/**6** equilibria was calculated to be fairly accessible at room temperature ($\Delta G^{\circ}_{\mathbf{1},\mathrm{diss}}$ = 0.2 kcal/mol, see SI Section XII).

The formation of **1** was found to be independent of applied potential, as even at mild potentials corresponding to the foot of the wave of the reduction of **2**, SEC experiments under N_2 still showed transient formation of **5^{t,t}** followed by the appearance of **1** (see SI Section XI). Accordingly, SEC experiments using **5^{t,t}** in place of **2** also generate **1** at the surface of the electrode, which aligns with reduction of **2** and **5^{t,t}** passing through the common intermediate, **3-N$_2$** (*vide supra*).

2.5 Role of Chemical Redox Reactions in N_2 Cleavage. *2.5.1 Detection of comproportionation reactions with electrode-generated Mo^0 species.* The observation that the dominant electrode-generated species are Mo^0 is highly surprising, as **1** is stable with respect to N_2 cleavage. Additionally, the detected yields of **1** after CPE are quite low (<2%), suggesting that it also serves as an intermediate in the N_2 cleavage reaction. This is supported by past reports of electrochemical N_2 cleavage at rhenium, wherein comproportionation-induced N_2 splitting (referred to simply as comproportionation hereafter) between starting material and over-reduced Re species was critical.[13,16] To determine whether similarly analogous transformations between **2** and Mo^0 species were feasible, IR, rR, and UV-Vis spectra were recorded in the absence of an applied potential immediately concluding stepped potential SEC experiments.

Monitoring the diffusion-limited reaction between surface-generated Mo^0 and bulk **2** in the starting material by IR spectroscopy revealed the rapid consumption of **1** followed by the slower consumption of **6** as a new transient feature appeared at 1932 cm^{-1} (**Figure 5B**). Similarly, rR monitoring revealed the consumption of **1** while features at

Scheme 4. Comproportionation reactions between [(^{py}PNP)Mo(N_2)$_2$]$_2$(μ-N_2) (**1**) and either (^{py}PNP)MoBr$_3$ (**2**) or *trans,trans*-[(^{py}PNP)Mo(N_2)Br$_2$]$_2$(μ-N_2) (**5^{t,t}**) in 0.2 M [^{n}Bu$_4$][PF_6] under N_2. Note that bimetallic species **1** and **5^{t,t}** are in equilibrium with monometallic **6** and **3**. Complex **7^{c,c}** is proposed to precede N_2 cleavage, but was not detected experimentally. Thermodynamic free energies (DG°) of comproportionation reactions to form 7c,c are included and account for the formation of 1.5 equiv (top) or 2 equiv (bottom) of 7c,c [a]Percent yield is obtained by dividing the concentration of **4** by the total concentration of all Mo atoms (see SI Section VI for an example calculation).

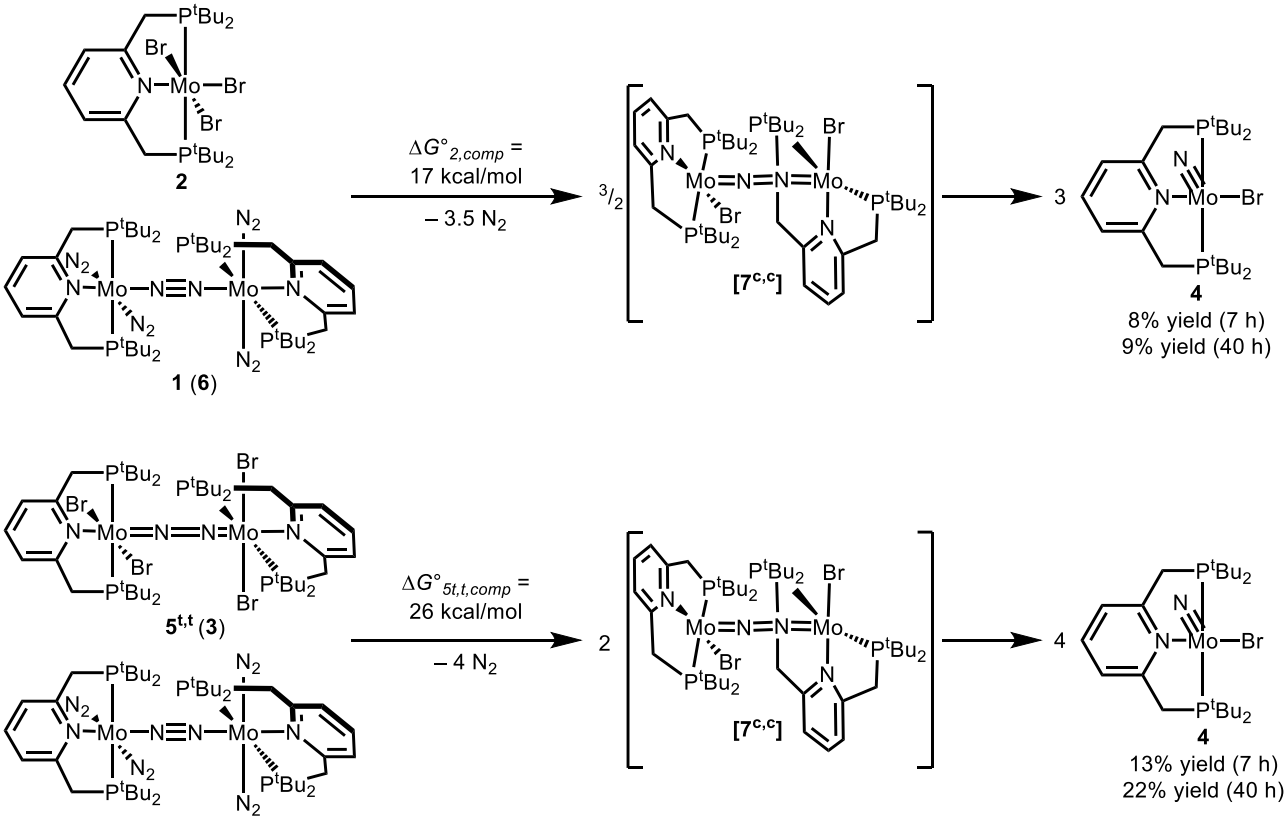

1595, 1680, and 1751 cm^{-1} returned, indicative of the formation of **5^{t,t}** (1595 and 1751 cm^{-1}) upon mixing of Mo^0 species and **2** (**Figure 5B**). The post-CPE UV-Vis also clearly revealed the formation of Mo^{II} species, as the bimodal λ_{max} features of **5^{t,t}** at 595 and 730 nm appeared over time. The observation of **5^{t,t}** also aligns with the detection of **5^{t,t}** in the bulk solution during CPE, as the stirring of the solution serves to increase the rate at which **1** generated at the electrode surface can react with unreduced **2**.

The reappearance of **5^{t,t}** after removal of an applied potential bias clearly demonstrates that comproportionation reactions are occurring in which **2** acts as a net Br$^•$ donor to **1**. This could subsequently generate key Mo^I species such as *cis,cis*-[(^{py}PNP)MoBr]$_2$(μ-N_2) (**7^{c,c}**, **Scheme 4** middle, here *cis* refers to the relationship between the bridging N_2 ligand and the pyridyl central donor) which is predicted to be the key intermediate preceding N_2 cleavage as it satisfies electronic and geometric structure rules.[13,23,42,44] Computations support this, as N_2 cleavage from **7^{c,c}** to form **4** is computed to be downhill by –48 kcal/mol (ΔG° = –24 kcal/mol per Mo(N) generated) with a kinetic barrier accessible at room temperature ($\Delta G^{‡}_{cleave}$ = 19 kcal/mol). The free energy of comproportionation of **1** and **2** to form **7^{c,c}** was computed to be only endergonic by 17 kcal/mol ($\Delta G°_{2,comp}$, **Scheme 4**, top).

The spectroscopic evidence for comproportionation of **1** and **2** in electrochemical reactions suggest a possible pathway for N_2 cleavage. To explore this further, chemical reactions between **1** and **2** were carried out starting from isolated Mo species to allow for NMR spectroscopy quantification of any Mo(N) products formed. These chemical reactions were carried out in 0.2 M [^{n}Bu$_4$N][PF_6] solutions in THF-d_8 to mimic the electrochemical medium. Upon addition of **2** to a green solution of **1**, a dark blue solution forms as **1** is completely consumed based on ^{1}H and ^{31}P{^{1}H} NMR spectroscopy. At the same time, the N_2 cleavage product **4** was detected in 8% spectroscopic yield at 7h (9% at 40 h). UV-Vis of the resultant solution revealed the dark blue color to be due to the formation of **5^{t,t}**, aligning with the SEC data and neither free ligand nor unidentifiable diamagnetic products were detected by ^{31}P{^{1}H} NMR spectroscopy.

The detection of **4** upon reaction of **1** and **2** indicates that comproportionation-induced N_2 cleavage reactions are a viable pathway during CPE of **2**. Having demonstrated that

Scheme 5. Proposed mechanisms for electroreductive N_2 cleavage by (^{py}PNP)$MoBr_3$ (**2**), with reactions that occur at the electrode surface (blue), reactions that occur in bulk solution (red), and reactions that occur in both locations (purple).

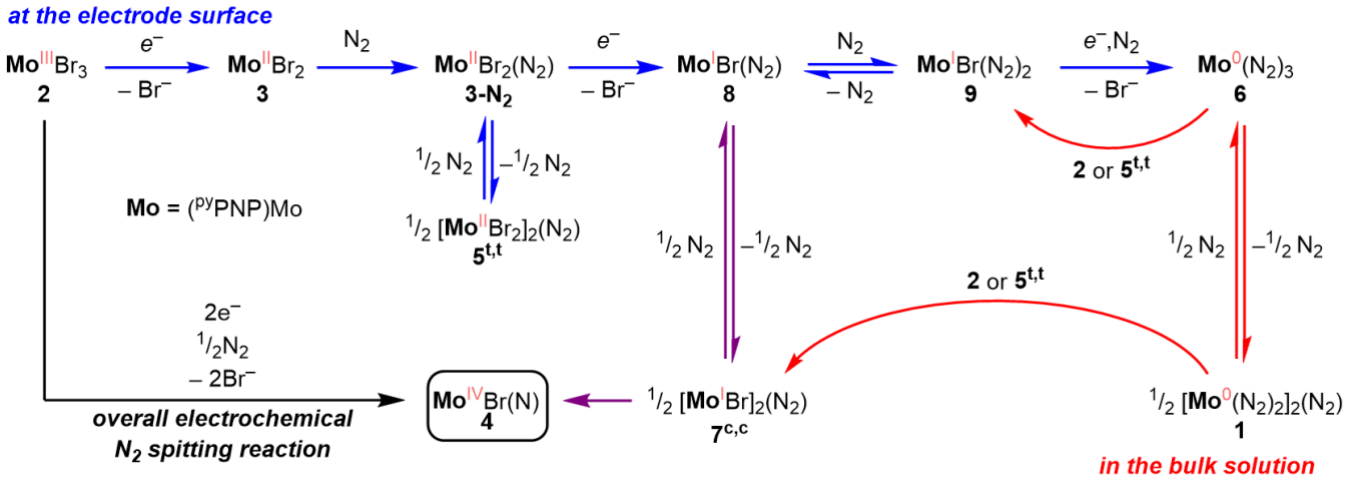

comproportionation of Mo^{III} and Mo^0 species was feasible, we next sought to determine whether the transient Mo^{II} species $\mathbf{5}^{t,t}$ could also participate in comproportionation reactions with Mo^0. Thus, under identical experimental conditions above, an isolated sample of $\mathbf{5}^{t,t}$ was added to a 0.2 M [^{n}Bu$_4$N][PF_6] solution in THF-d_8 containing **1**. While no immediate color change was observed, **4** was detected by ^{1}H NMR spectroscopy (13% at 7h, 22% at 40 h). Computational analysis of this transformation once again revealed that initial comproportionation to form $\mathbf{7}^{c,c}$ is uphill ($\Delta G^\circ_{\mathbf{5t,t},comp}$ = 26 kcal/mol, for 2 equivalents of $\mathbf{7}^{c,c}$) followed by highly exergonic N_2 splitting (**Scheme 4,** bottom).

These results unequivocally show that comproportionation reactions between low-valent Mo^0 species and both Mo^{II} and Mo^{III} species are capable of driving N_2 cleavage reactions. The observation of this chemically-driven oxidation of **1** resulting in N_2 splitting is reminiscent of the recently reported (electro)oxidation-induced N_2 cleavage by *trans*-(depe)$_2$Mo(N_2)$_2$.[15] Further contextualized with previous studies of (PNP)Re electroreductive N_2 cleavage,[13,16] these results suggest that over-reduction and subsequent comproportionation may be quite common in N_2 splitting mechanisms. Additionally, it is important to note that these chemical redox reactions are sufficiently slow so that they are only observed *away* from the electrode surface,[47] suggesting that the spatial separation afforded by an electrochemical approach (i.e. electrode equivalents only available at the electrode surface) is playing a critical role in the overall mechanism.

2.5.2 Implications for N_2 fixation catalysis. The ability of **2** and $\mathbf{5}^{t,t}$ to act as chemical oxidants capable of drawing Mo^0 species onto the N_2 splitting pathway led us to consider other oxidation reactions. One particularly relevant transformation would be the oxidative protonation of Mo^0 species, as molecular acids are already used during N_2 fixation catalysis. Previously, protonation of **1** with HBF_4•Et_2O in the presence of pyridine resulted in isolation of a hydrazido complex supported by an additional pyridine ligand.[18] The formation of a Mo(N) product was not reported. Herein, we targeted similar reactivity but used [HLut][Br], with the sterically bulky lutidine chosen to avoid coordination and the bromide counteranion chosen to promote generation of the nitrido bromide complex **4**.

Upon addition of one equivalent of [HLut][Br] to a THF-d_8 solution of **1**, complex **1** was completely consumed and **4** could be detected in 40% yield by ^{1}H NMR spectroscopy. No NH_4^+ was detected, suggesting that the nitride did not originate from NH_3 release upon protonation of a distal nitrogen atom. This demonstrates that protonation is a viable pathway to convert low-valent Mo^0 species to more reactive Mo(N) intermediates via N_2 splitting. The site of protonation of a low-valent N_2 complex can be thought of as setting the N_2 fixation pathway: protonation at the distal nitrogen of a terminal N_2 ligand would lead to a distal (or alternating) mechanism, while protonation at the metal center can increase the formal oxidation state and lead to N_2 cleavage pathways for N_2 fixation.

2.6 Constructing Pathways of Electrochemical N_2 Cleavage. The combined electrochemical and spectroscopic data are consistent with *two concurrent and interconnected pathways* for electrochemical N_2 cleavage by (PNP)$MoBr_3$ (**2**). As shown in **Scheme 5**, one pathway takes place entirely in the vicinity of the electrode surface, while the other pathway features comproportionation chemical redox reactions that generate **4** away from the electrode surface. This spatial separation of different reaction pathways is a consequence of the inherent heterogeneity of electron transfer reactions at solid electrode surfaces.

The initial reductive N_2 activation steps, which occur near the electrode surface, are identical for the two pathways. Cyclic voltammetry studies establish that reduction of **2** triggers Br^- dissociation to generate the 5-coordinate species (^{py}PNP)$MoBr_2$ (**3**, **Scheme 5**, $\Delta G^\circ_{Br,diss}$ = –2 kcal/mol). N_2 association to **3** generates **3-N$_2$** (for *cis*-**3-N$_2$**, $\Delta G^\circ_{N2binding}$ = 6 kcal/mol; for *trans*-**3-N$_2$**, $\Delta G^\circ_{N2binding}$ = 7

kcal/mol), which is in equilibrium with the bimetallic species *trans,trans*-[(^{py}PNP)MoBr$_2$]$_2$(μ-N$_2$) and free N$_2$ (**5^{t,t}**, **Scheme 5**). The monometallic-bimetallic equilibrium heavily favors **5^{t,t}** ($\Delta G^\circ_{dimerization}$ = −4 or −5 kcal/mol depending on isomer of **3-N$_2$**), consistent with the detection of **5^{t,t}** at the electrode surface during SEC experiments.

Although **5^{t,t}** is the dominant Mo^{II} species, this complex has a highly negative reduction potential, and electrolysis at such negative potentials results in significantly decreased yields of **4** (**Table 1**, above). The monometallic-bimetallic equilibrium is therefore essential because it enables subsequent reduction to proceed via a CE mechanism: in a chemical step, **5^{t,t}** dissociates to generate one equivalent of **3-N$_2$**, which is reduced at milder potentials than **5^{t,t}**. This CE process also explains why N$_2$ cleavage can be observed under Ar when starting from **5^{t,t}**, as reduction of **3-N$_2$** remains accessible even in the absence of an N$_2$ headspace. Once **3-N$_2$** is reduced at the electrode surface, subsequent loss of a bromide anion generates the 5-coordinate Mo^{I} species (^{py}PNP)MoBr(N$_2$) (**8**, **Scheme 6**).

After formation of **8**, the two concurrent reaction pathways bifurcate. Focusing first on the bulk solution pathway observed under N$_2$, coordinatively unsaturated **8** can bind a second equivalent of N$_2$ to form *trans*-(^{py}PNP)MoBr(N$_2$)$_2$ (**9**, **Scheme 6**, $\Delta G^\circ_{N2binding}$ = −8 kcal/mol and $\Delta G^{\ddagger}_{N2binding}$ = 10 kcal/mol). Support for the formation of **9** arises from the recently reported isolation of *trans*-(^{py}PNP)MoI(N$_2$)$_2$ as a precursor to N$_2$ cleavage when warmed above −30 °C.[27]

Scheme 6. Stepwise formation of (^{py}PNP)Mo(N)Br (**4**) at the electrode surface upon reduction of (^{py}PNP)MoBr$_2$(N$_2$) (**3-N$_2$**).

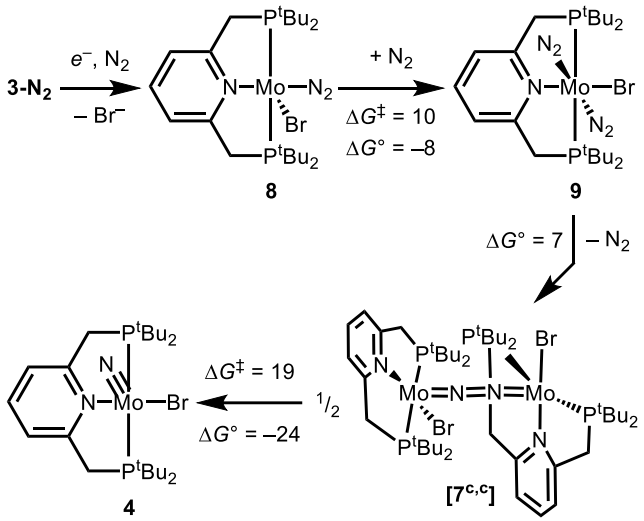

After formation of **9**, the Mo^{I} species is further reduced at the electrode surface to yield the bimetallic Mo^0 species, **1**. Complex **1** and its monometallic equilibrium partner (^{py}PNP)Mo(N$_2$)$_3$ (**6**) are found to be the dominant Mo species detected by UV-vis, IR, and rR SEC experiments (**Scheme 5**) and do not cleave N$_2$ to form Mo(N) products. However, as the Mo^0 species diffuse away from the electrode into the bulk solution, they can participate in chemical redox reactions with **2** or **5^{t,t}** via comproportionation to generate the bimetallic Mo$^{I/I}$ complex *cis,cis*-[(^{py}PNP)MoBr]$_2$(μ-N$_2$) (**7^{c,c}**, **Scheme 5**, $\Delta G^\circ_{2,comp}$= 11 kcal/mol per equivalent of **7^{c,c}** formed). Subsequent N–N bond cleavage from **7^{c,c}** to yield **4** was computed to be kinetically accessible ($\Delta G^{\ddagger}_{cleave}$ = 19 kcal/mol) and thermodynamically favorable (ΔG°_{cleave} = −24 kcal/mol). Yoshizawa and Nishibayashi have proposed that the iodide analogue of **7^{c,c}** is the species responsible for N$_2$ cleavage in the reduction of N$_2$ to give ammonia catalyzed by (^{py}PNP)MoI$_3$.[27]

Experimental support for the bulk solution pathway arises from time courses showing that **1** reacts after the applied potential is released in SEC experiments, and from chemical comproportionation reactions of **1** and either **2** or **5^{t,t}**, which form **4** in the absence of an applied potential. These chemical redox pathways can "rescue" over-reduced Mo complexes to generate the Mo^{I} intermediates active for N$_2$ splitting. However, the over-reduction to Mo^0 species in the bulk solution pathway cannot explain the electrochemical N$_2$ splitting observed under Ar (**Table 1**). Furthermore, mixing isolated samples of **1** with either **2** or **5^{t,t}** leads only to low yields of **4**. These observations therefore indicate that a second pathway must be operating in tandem.

Returning to the key intermediate **8**, a second pathway proceeding within the reaction-diffusion layer near the electrode surface is also operable. Under Ar, **8** can directly rearrange to generate the N$_2$-bridged complex **7^{c,c}** while under N$_2$, further equilibrium with the monometallic **9** is likely occurring (**Scheme 5**). The conversion of **9** to **7^{c,c}** is calculated to be only slightly uphill ($\Delta G^\circ_{formation}$ = 7 kcal/mol, **Scheme 6**) with subsequent N$_2$ cleavage leading to an overall exothermic process. This pathway must be viable because reduction of **5^{t,t}** under an Ar atmosphere yields **4**. Under Ar, there is no N$_2$ available to support over-reduction to **1**, thus precluding any chemical redox reactions. In support of this mechanism proceeding solely at the electrode surface, a feature consistent with **4** appears in the return sweep of CVs of **5^{t,t}** under both Ar and N$_2$, consistent with N$_2$ splitting in the reaction layer (**Figure S57**).

The two pathways for electrochemical N$_2$ splitting are likely both operating during electrolysis. The dominant path under N$_2$ will depend on the relative rate of (a) the chemical formation of **7^{c,c}** from **8** or **9**, and (b) the electrochemical reduction of **9** to Mo^0 complexes **6** and **1**. A change in dominant nitride synthesis path may be reflected in the data of **Table 1** (above). For example, the yields of **4** drop considerably when more negative applied potentials are employed, suggesting that the pathway involving over-reduction followed by comproportionation is predominantly responsible for generating **4**. Conversely, the yield of **4** is higher when N$_2$-bridged complex **5^{t,t}**

undergoes CPE under Ar (with N_2 splitting at the electrode surface) than under N_2 (where over-reduction necessitates chemical redox pathways).

3. CONCLUSIONS

The viability of electrochemical N_2 binding and splitting by the molybdenum(III) pincer complex, (^{py}PNP)$MoBr_3$ is established in this work. The N_2-derived nitride (^{py}PNP)Mo(N)Br was actually produced in higher yields during electrolysis (41%) than when chemical reductants were used (20%). Employing a suite of electrochemical, spectroscopic, and computational methods provides a detailed account of the electroreductive N_2 splitting mechanisms: initial reduction of (^{py}PNP)$MoBr_3$ generates Mo^{I} species at the electrode surface that can either (a) form N_2-bridged intermediates that cleave N_2 in the reaction–diffusion layer near the electrode surface, or (b) be further electroreduced to Mo^0 species that undergo *chemical* redox reactions with higher-valent Mo species to generate the desired nitride product in the bulk solution. These comproportionation reactions can be directly observed in the bulk solution, far from the electrode surface, in the absence of an applied potential.

The electrochemical yield of (^{py}PNP)Mo(N)Br was found to be strongly dependent on applied potential, with higher yields of nitride obtained at less negative potentials. Two key mechanistic features contribute to this observation: first is the potential inversion that occurs upon binding of N_2, which helps lower the necessary applied potential for the second and third electron transfer events. Secondly, the presence of rapid monometallic-bimetallic complex equilibria plays a role. At more negative potentials, bimetallic Mo^{II} species can be reduced directly, and the resulting Mo^{I} species are rapidly converted to Mo^0 (perhaps because they are in a *trans,trans* geometry coming from $\mathbf{5^{t,t}}$, slowing the rate of N_2 splitting) — thereby precluding N_2 splitting at the electrode surface.

Another distinct feature of the discovered electrochemical mechanism of N_2 cleavage is the spatial evolution of the reaction. Near the electrode surface, Mo^{I} species face a kinetic competition between (a) formation of the N_2-bridged intermediate capable of splitting into nitride complexes, and (b) over-reduction to Mo^0 species. Once Mo^0 species are generated, no further reaction at the electrode surface is possible. As the Mo^0 species diffuse away from the electrode and into the bulk solution, however, chemical redox reactions with starting material can take place to re-form Mo^{I} species and eventually split N_2. It is not without irony that an "electrochemical" N_2 splitting reaction relies on a chemical redox reaction! This also provides a key lesson for future electrochemical mechanistic investigations: researchers cannot solely focus on reactions occurring within the reaction layer near the electrode surface. Spectroscopic probes both near the electrode surface and in the bulk solution can provide complementary mechanistic insights during electrolyses. These considerations are also relevant more broadly in electrochemistry that involves chemical redox reactions, particularly mediated electrocatalysis.[12,48]

The intermediacy of Mo^0 complex **1** in an N_2 splitting pathway also raises important questions about mechanisms of ammonia synthesis. We have shown that either chemical oxidants (Mo^{III} or Mo^{II} species) or a lutidinium acid commonly used in catalytic N_2 fixation can react with **1** to generate (^{py}PNP)Mo(N)Br. Complex **1** is representative of a wide class of low-valent Mo complexes that have been proposed to reduce N_2 via the so-called "distal pathway" first proposed by Chatt. Mechanistic studies demonstrate that **1** can participate in an N_2 splitting pathway.

Demonstrating electrochemical N_2 splitting at molybdenum ultimately led us to elucidate unanticipated mechanistic aspects that can guide catalyst development.

ASSOCIATED CONTENT

Supporting Information

Experimental details and characterization data (PDF)
Coordinates of optimized geometries in compressed .mol format (ZIP)

Accession codes

CCDC 2106759 contains the supplementary crystallographic data for this paper. This datum can be obtained free of charge via www.ccdc.cam.ac.uk/data_request/cif, or by emailing data_request@ccdc.cam.ac.uk, or by contacting The Cambridge Crystallographic Data Centre, 12 Union Road, Cambridge CB2 1EZ, UK; fax: +44 1223 336033.

AUTHOR INFORMATION

Corresponding Author

* A.J.M.M. Email: ajmm@email.unc.edu

ACKNOWLEDGMENTS

The experimental and computational work was supported through the NSF Chemical Catalysis program under Grants No. CHE-1954942 and CHE-1955014. Q.J.B. acknowledges support from the NSF Graduate Research Fellowship Program (DGE-1650116) and the UNC Dissertation Completion Fellowship Program. The authors thank Prof. Joanna Atkin for assistance with designing spectroelectrochemical resonance Raman experiments. The authors also thank Prof. Jillian Dempsey for assistance with CV simulation. The mass spectrometry work was supported by the National Science Foundation under Grant No. (CHE-1726291). A portion of this work was performed using the Renishaw inVia Raman microscope in the CHASE Instrumentation facility established by the Center for Hybrid Approaches in Solar Energy to Liquid Fuels (CHASE), an Energy Innovation Hub funded by the U.S. Department of Energy, Office of Science, Office of Basic Energy Sciences under Award Number DE-SC0021173. The

NMR spectroscopy work was supported by the National Science Foundation under Grant No. CHE-1828183.

REFERENCES

(1) Vaclav, S. Detonator of the Population Explosion. *Nature* **1999**, *400*, 415.

(2) Erisman, J. W.; Sutton, M. A.; Galloway, J.; Klimont, Z.; Winiwarter, W. How a Century of Ammonia Synthesis Changed the World. *Nat. Geosci.* **2008**, *1*, 636–639.

(3) Renner, J. N.; Greenlee, L. F.; Herring, A. M.; Ayers, K. E. Electrochemical Synthesis of Ammonia: A Low Pressure, Low Temperature Approach. *Electrochem. Soc. Interface* **2015**, *24*, 51–57.

(4) Tallaksen, J.; Bauer, F.; Hulteberg, C.; Reese, M.; Ahlgren, S. Nitrogen Fertilizers Manufactured Using Wind Power: Greenhouse Gas and Energy Balance of Community-Scale Ammonia Production. *J. Clean. Prod.* **2015**, *107*, 626–635.

(5) Hochman, G.; Goldman, A.; Felder, F. A.; Mayer, J.; Miller, A.; Holland, P. L.; Goldman, L.; Manocha, P.; Song, Z.; Aleti, S. The Potential Economic Feasibility of Direct Electrochemical Nitrogen Reduction as a Route to Ammonia. *ACS Sustain. Chem. Eng.* **2020**, *8*, 8938–8948.

(6) Dmitry V. Yandulov; Schrock, R. R. Catalytic Reduction of Dinitrogen to Ammonia at a Single Molybdenum Center. *Science* **2003**, *301*, 76–78.

(7) Eizawa, A.; Nishibayashi, Y. Catalytic Nitrogen Fixation Using Molybdenum–Dinitrogen Complexes as Catalysts. In *Topics in Organometallic Chemistry*; Springer Verlag, 2017; Vol. 60, pp 153–169.

(8) Ashida, Y.; Nishibayashi, Y. Catalytic Conversion of Nitrogen Molecule into Ammonia Using Molybdenum Complexes under Ambient Reaction Conditions. *Chem. Commun.* **2021**, *57*, 1176–1189.

(9) Bennaamane, S.; Espada, M. F.; Mulas, A.; Personeni, T.; Saffon-Merceron, N.; Fustier-Boutignon, M.; Bucher, C.; Mézailles, N. Catalytic Reduction of N_2 to Borylamine at a Molybdenum Complex. *Angew. Chem. Int. Ed.* **2021**, *60*, 20210–20214.

(10) Tanabe, Y.; Nishibayashi, Y. Comprehensive Insights into Synthetic Nitrogen Fixation Assisted by Molecular Catalysts under Ambient or Mild Conditions. *Chem. Soc. Rev.* **2021**, *50*, 5201–5242.

(11) Pickett, C. J.; Talarmin, J. Electrosynthesis of Ammonia. *Nature* **1985**, *317*, 652–653.

(12) Chalkley, M. J.; Del Castillo, T. J.; Matson, B. D.; Peters, J. C. Fe-Mediated Nitrogen Fixation with a Metallocene Mediator: Exploring PK_a Effects and Demonstrating Electrocatalysis. *J. Am. Chem. Soc.* **2018**, *140*, 6122–6129.

(13) Lindley, B. M.; van Alten, R. S.; Finger, M.; Schendzielorz, F.; Würtele, C.; Miller, A. J. M.; Siewert, I.; Schneider, S. Mechanism of Chemical and Electrochemical N_2 Splitting by a Rhenium Pincer Complex. *J. Am. Chem. Soc.* **2018**, *140*, 7922–7935.

(14) Sherbow, T. J.; Thompson, E. J.; Arnold, A.; Sayler, R. I.; Britt, R. D.; Berben, L. A. Electrochemical Reduction of N_2 to NH_3 at Low Potential by a Molecular Aluminum Complex. *Chem. – A Eur. J.* **2019**, *25*, 454–458.

(15) Katayama, A.; Ohta, T.; Wasada-Tsutsui, Y.; Inomata, T.; Ozawa, T.; Ogura, T.; Masuda, H. Dinitrogen-Molybdenum Complex Induces Dinitrogen Cleavage by One-Electron Oxidation. *Angew. Chem. Int. Ed.* **2019**, *58*, 11279–11284.

(16) van Alten, R. S.; Wätjen, F.; Demeshko, S.; Miller, A. J. M.; Würtele, C.; Siewert, I.; Schneider, S. (Electro-)Chemical Splitting of Dinitrogen with a Rhenium Pincer Complex. *Eur. J. Inorg. Chem.* **2020**, *2020*, 1402–1410.

(17) Garrido-Barros, P.; Derosa, J.; Chalkley, M. J.; Peters, J. C. Tandem Electrocatalytic N_2 Fixation via Concerted Proton-Electron Transfer. *ChemRxiv* **2021**.

(18) Arashiba, K.; Miyake, Y.; Nishibayashi, Y. A Molybdenum Complex Bearing PNP-Type Pincer Ligands Leads to the Catalytic Reduction of Dinitrogen into Ammonia. *Nat. Chem.* **2011**, *3*, 120–125.

(19) Chatt, J. A Possible Mimic of the Nitrogenase Reaction. In *Biomimetic Chemistry*; American Chemical Society, 1980; pp 379–391.

(20) Schrock, R. R. Catalytic Reduction of Dinitrogen to Ammonia at a Single Molybdenum Center. *Acc. Chem. Res.* **2005**, *38*, 955–962.

(21) Tanaka, H.; Arashiba, K.; Kuriyama, S.; Sasada, A.; Nakajima, K.; Yoshizawa, K.; Nishibayashi, Y. Unique Behaviour of Dinitrogen-Bridged Dimolybdenum Complexes Bearing Pincer Ligand towards Catalytic Formation of Ammonia. *Nat. Commun. 2014 51* **2014**, *5*, 1–11.

(22) Kuriyama, S.; Arashiba, K.; Nakajima, K.; Tanaka, H.; Kamaru, N.; Yoshizawa, K.; Nishibayashi, Y. Catalytic Formation of Ammonia from Molecular Dinitrogen by Use of Dinitrogen-Bridged Dimolybdenum-Dinitrogen Complexes Bearing PNP-Pincer Ligands: Remarkable Effect of Substituent at Pnp-Pincer Ligand. *J. Am. Chem. Soc.* **2014**, *136*, 9719–9731.

(23) Arashiba, K.; Eizawa, A.; Tanaka, H.; Nakajima, K.; Yoshizawa, K.; Nishibayashi, Y. Catalytic Nitrogen Fixation via Direct Cleavage of Nitrogen–Nitrogen Triple Bond of Molecular Dinitrogen under Ambient Reaction Conditions. *Bull. Chem. Soc. Jpn.* **2017**, *90*, 1111–1118.

(24) Ashida, Y.; Arashiba, K.; Nakajima, K.; Nishibayashi, Y. Molybdenum-Catalysed Ammonia Production with Samarium Diiodide and Alcohols or Water. *Nature* **2019**, *568*, 536–540.

(25) Elgrishi, N.; Kurtz, D. A.; Dempsey, J. L. Reaction Parameters Influencing Cobalt Hydride Formation Kinetics: Implications for Benchmarking H_2-Evolution Catalysts. *J. Am. Chem. Soc.* **2017**, *139*, 239–244.

(26) Savéant, J.; Costentin, C. Elements of Molecular and Biomolecular Electrochemistry; Wiley, 2019.

(27) Arashiba, K.; Tanaka, H.; Yoshizawa, K.; Nishibayashi, Y. Cycling between Molybdenum-Dinitrogen and -Nitride Complexes to Support the Reaction Pathway for Catalytic Formation of Ammonia from Dinitrogen. *Chem. – A Eur. J.* **2020**, *26*, 13383–13389.

(28) Al-Salih, T. I.; Pickett, C. J. Electron-Transfer Reactions in Nitrogen Fixation. Part 1. The Electrosynthesis of Dinitrogen, Hydride, Isocyanide, and Carbonyl Complexes of Molybdenum: Intermediates, Mechanisms, and Energetics. *J. Chem. Soc. Dalt. Trans.* **1985**, *53*, 1255.

(29) Kirchhoff, J. R.; Heineman, W. R.; Deutsch, E. Technetium Electrochemistry. 4. Electrochemical And Spectroelectrochemical Studies On The Bis(Tertiary Phosphine Or Arsine (D))Rhenium(III) Complexes Trans - $[Red_2X_2]+$ (X = Cl, Br). Comparison With The Technetium(III) Analogues. *Inorg. Chem.* **1987**, *26*, 3108–3113.

(30) Lever, A. B. P. Electrochemical Parametrization of Rhenium Redox Couples. *Inorg. Chem.* **1991**, *30*, 1980–1985.

(31) Peters, J. C.; Cherry, J.-P. F.; Thomas, J. C.; Baraldo, L.; Mindiola, D. J.; Davis, W. M.; Cummins, C. C. Redox-Catalyzed Binding of Dinitrogen by Molybdenum N - Tert - Hydrocarbylanilide Complexes: Implications for Dinitrogen Functionalization and Reductive Cleavage. *J. Am. Chem. Soc.* **1999**, *121*, 10053–10067.

(32) Rittle, J.; McCrory, C. C. L.; Peters, J. C. A 10^6-Fold Enhancement in N_2-Binding Affinity of an $Fe_2(\mu\text{-}H)_2$ Core upon Reduction to a Mixed-Valence $Fe^{II}Fe^{I}$ State. *J. Am. Chem. Soc.* **2014**, *136*, 13853–13862.

(33) Clouston, L. J.; Bernales, V.; Carlson, R. K.; Gagliardi, L.; Lu, C. C. Bimetallic Cobalt-Dinitrogen Complexes: Impact of the Supporting Metal on N_2 Activation. *Inorg. Chem.* **2015**, *54*, 9263–9270.

(34) Del Castillo, T. J.; Thompson, N. B.; Peters, J. C. A Synthetic Single-Site Fe Nitrogenase: High Turnover, Freeze-Quench ^{57}Fe Mössbauer Data, and a Hydride Resting State. *J. Am. Chem. Soc.* **2016**, *138*, 5341–5350.

(35) Bezdek, M. J.; Guo, S.; Chirik, P. J. Terpyridine Molybdenum Dinitrogen Chemistry: Synthesis of Dinitrogen Complexes That Vary by Five Oxidation States. *Inorg. Chem.* **2016**, *55*, 3117–3127.

(36) Rafiq, S.; Bezdek, M. J.; Chirik, P. J.; Scholes, G. D. Dinitrogen Coupling to a Terpyridine-Molybdenum Chromophore Is Switched on by Fermi Resonance. *Chem* **2019**, *5*, 402–416.

(37) Arashiba, K.; Kuriyama, S.; Nakajima, K.; Nishibayashi, Y. Preparation and Reactivity of a Dinitrogen-Bridged Dimolybdenum-Tetrachloride Complex. *Chem. Commun.* **2013**, *49*, 11215–11217.

(38) Holland, P. L. Metal-Dioxygen and Metal-Dinitrogen Complexes: Where Are the Electrons? *Dalton Trans.* **2010**, *39*, 5415–5425.

(39) Cui, Q.; Musaev, D. G.; Svensson, M.; Sieber, S.; Morokuma, K. N_2 Cleavage by Three-Coordinate Group 6 Complexes. W(III) Complexes Would Be Better Than Mo(III) Complexes. *J. Am. Chem. Soc.* **1995**, *117*, 12366–12367.

(40) Laplaza, C. E.; Johnson, M. J. A.; Peters, J. C.; Odom, A. L.; Kim, E.; Cummins, C. C.; George, G. N.; Pickering, I. J. Dinitrogen Cleavage by Three-Coordinate Molybdenum(III) Complexes: Mechanistic and Structural Data. *J. Am. Chem. Soc.* **1996**, *118*, 8623–8638.

(41) Bruch, Q. J.; Connor, G. P.; McMillion, N. D.; Goldman, A. S.; Hasanayn, F.; Holland, P. L.; Miller, A. J. M. Considering Electrocatalytic Ammonia Synthesis via Bimetallic Dinitrogen Cleavage. *ACS Catal.* **2020**, *10*, 10826–10846.

(42) Yamout, L. S.; Ataya, M.; Hasanayn, F.; Holland, P. L.; Miller, A. J. M.; Goldman, A. S. Understanding Terminal versus Bridging End-on N_2 Coordination in Transition Metal Complexes. *J. Am. Chem. Soc.* **2021**, *143*, 9744–9757.

(43) Krejčik, M.; Daněk, M.; Hartl, F. Simple Construction of an Infrared Optically Transparent Thin-Layer Electrochemical Cell. Applications to the Redox Reactions of Ferrocene, $Mn_2(CO)_{10}$ and $Mn(CO)_3$ (3,5-Di-t-Butyl-Catecholate)$^-$. *J. Electroanal. Chem. Interfacial Electrochem.* **1991**, *317*, 179–187.

(44) Bruch, Q. J.; Connor, G. P.; Chen, C.-H.; Holland, P. L.; Mayer, J. M.; Hasanayn, F.; Miller, A. J. M. Dinitrogen Reduction to Ammonium at Rhenium Utilizing Light and Proton-Coupled Electron Transfer. *J. Am. Chem. Soc.* **2019**, *141*, 20198–20208.

(45) Liao, Q.; Saffon-Merceron, N.; Mézailles, N. N_2 Reduction into Silylamine at Tridentate Phosphine/Mo Center: Catalysis and Mechanistic Study. *ACS Catal.* **2015**, *5*, 6902–6906.

(46) Kuriyama, S.; Arashiba, K.; Nakajima, K.; Tanaka, H.; Yoshizawa, K.; Nishibayashi, Y. Azaferrocene-Based PNP-Type Pincer Ligand: Synthesis of Molybdenum, Chromium, and Iron Complexes and Reactivity toward Nitrogen Fixation. *Eur. J. Inorg. Chem.* **2016**, *2016*, 4856–4861.

(47) Mastragostino, M.; Nadjo, L.; Saveant, J. M.

Disproportionation and ECE Mechanisms—I. Theoretical Analysis. Relationships for Linear Sweep Voltammetry. *Electrochim. Acta* **1968**, *13*, 721–749.

(48) Anson, C. W.; Stahl, S. S. Mediated Fuel Cells: Soluble Redox Mediators and Their Applications to Electrochemical Reduction of O2 and Oxidation of H2, Alcohols, Biomass, and Complex Fuels. *Chem. Rev.* **2020**, *120*, 3749–3786.